Klemann, V., Martinec, Z. (2009): Contribution of glacial-isostatic adjustment to the geocenter motion. - Tectonophysics, 511, 3-4, 99-108

DOI: 10.1016/j.tecto.2009.08.031

# Contribution of glacial-isostatic adjustment to the geocenter motion

Volker Klemann*[1] and Zdeněk Martinec[1,2]

[1] Helmholtz Center Potsdam, German Research Center for Geosciences, Sect. 1.5: Earth System Modelling, Telegrafenberg, D-14473 Potsdam, Germany

[2] Charles University, v Holešovičkách 2, 180 00 Prague 8, Czech Republic

* corresponding author (volkerk@gfz-potsdam.de)

Short title: Geocenter motion due to GIA

## Abstract

The geocenter motion describes the surface net-displacement of the entire solid Earth with respect to the center of mass of the entire Earth including surface masses. Therefore, it resembles an integrative quantity of surface displacement and mass redistribution inside the Earth as well as at its surface. Seasonal variations of this quantity are understood to originate mainly from mass redistribution in the water cycle. In contrast, a secular trend of the geocenter motion is possible to result also from the dynamics of the Earth's interior. One mechanism inducing a secular geocenter motion is the glacial-isostatic adjustment, describing the deformation and mass redistribution in the Earth's interior due to glaciations during the Pleistocene. Focusing on this contribution, we compute the geocenter motion from the displacement and gravity-potential fields calculated for a spherical, self-gravitating, incompressible and viscoelatic Earth model loaded by the last Pleistocene glacial cycle. We discuss the fluid-core approximation usually adopted and assess the influence of a list of modelling parameters which are the upper- and lower-mantle viscosity, lithosphere thickness, and glaciation history. We find a rather robust geocenter motion with respect to parameter variations, which is directed towards Northeast Canada and shows velocities that vary between 0.1 and 1 mm/yr depending on the adopted Earth-model and glaciation-history parameterisations.

# 1 Introduction

Due to increasing accuracy in determining the Earth-orientation parameters, the geocenter (GC) motion becomes more important. We define it here according to Blewitt (2003) as the motion of the center of figure (CF), i.e. the 'frame defined geometrically as though the Earth's surface were covered by a uniform, infinitely dense array of points', against the center of mass (CM) of the entire Earth system including surface masses. Whereas the variations of surface masses in ocean, atmosphere, cryosphere and continental hydrology contribute the largest seasonal signal (e.g. Chen *et al.*, 1999) long term variations can also be explained by mass redistributions in the Earth's interior.

The GC motion can be determined from combination of observations like DORIS and LAGEOS (e.g. Bouillé *et al.*, 2000), using GRACE tracking data (Kang *et al.*, 2009), VLBI or GPS. A problem of this combination of ground-based and satellite data is the unequal distribution of observation points at the Earth's surface. As discussed in Blewitt (2003), a fiducial-free network displacement of GPS-stations should be possible to use for geodynamic constraints, if all non-gravitational forces contaminating the motion of the satellites would be known (Heflin *et al.*, 1992). The seasonal signal is determined rather accurately (Dong *et al.*, 2003; Blewitt *et al.*, 2001; Lavallée *et al.*, 2006) and its origin from the redistribution of surface masses is understood (Chen *et al.*, 1999; Wu *et al.*, 2006). The secular trend of the GC motion can also result from mass redistribution in the Earth's interior. As already suggested by Greff-Lefftz (2000), one candidate is the glacial-isostatic adjustment (GIA) which describes the adjustment of the Earth's interior after the last glacial cycle which terminated 8,000 yr before present.

Recently, Argus (2007) assessed the contribution of GIA to this motion to be not larger than 0.1 mm/yr. He considered the main effect of GIA on the GC motion to be the mass change due to the uplift in Laurentide, determined this as a motion of the solid-Earth system (CE) against the CM according to Blewitt *et al.* (2001) and got a velocity of 0.034 mm/yr for the Earth-model/glaciation-history combination VM2/ICE-5G (Peltier, 2004). Determining the GIA-induced GC motion from the global surface displacement field, Greff-Lefftz (2000) studied the dependence of GC motion on the viscosity contrast between upper and lower mantle and predicted values of up to 0.4 mm/yr, where she considered the glaciation history ICE3G (Tushingham & Peltier, 1991). Further more, applying a formal inversion, Wu *et al.* (2009) assessed a value of 0.7 mm/yr for the contribution of GIA.

Based on the numerical technique of Martinec (2000), we revisit the calculation of the GC motion for a viscoelastic non-rotating planet and present the uniqueness conditions for determining the GIA-induced deformation.

Furthermore, we discuss the influence of the fluid-core approximation, often applied in modelling of GIA. This approximation considers the influence of the fluid core as a boundary condition at the core-mantle boundary assuming the core as a self-gravitating fluid persisting to remain in a hydrostatic state (Crossley & Gubbins, 1975). The presented model is applied to Earth-model/glaciation-history combinations, the influence of lower- and upper-mantle viscosity on GC motion is discussed and the influence of the chosen glaciation history is shown.

The study is based on the solution strategy of solving the field equations with a spectral finite element method (SFEM) suggested by Martinec (2000). There, the radial dependence of the fields are solved by finite elements whereas the lateral dependence is set up in spherical harmonics. The time dependence of the viscous flow is solved directly in the time domain omitting the usually considered normal mode theory in the Laplace domain (Wu & Peltier, 1982). Due to the chosen set up of the system of equations and in addition to boundary conditions which resemble the loading process, six uniqueness conditions have to be specified. In order to prohibit a net translation, the usual choice is to consider the CM or, alternatively, to consider the CF to be invariant with respect to the loading process. A second set of uniqueness conditions is related to the rotation of the body. Here we consider the ITRF convention of no surface net rotation (e.g. Kreemer *et al.*, 2006).

In this study, we aim at emphasizing a significant influence of lower-mantle viscosity on a GC motion. The Earth-model/glaciation-history combination VM2/ICE-5G of Peltier (2004) results in a GC motion of about 0.1 mm/yr (Argus, 2007), which can partly be explained by a small lower-mantle viscosity considered in VM2. Predictions of the $\dot{J}_2$-term by GIA and comparison to true polar wander suggest a significant viscosity contrast between upper and lower mantle of at least one order of magnitude (Vermeersen *et al.*, 1998). Furthermore, Greff-Lefftz (2000) already showed that considering the glaciation history ICE3G (Tushingham & Peltier, 1991) and a viscosity contrast of 10 between lower and upper mantle amplifies the GC motion to 0.5 mm/yr.

## 2 Theoretical background

Since the viscoelastic response of the Earth induced by glacial loading has a global feature, it is convenient to treat it in spherical coordinates and parameterize field variables in terms of surface spherical harmonics. Such a parameterization is used, for instance, in Peltier (1974), Wu & Peltier (1982) and Martinec (2000). Here, we introduce the representation of the Eulerian gravitational-potential increment, $\phi^E$, and the displacement vector, $\boldsymbol{u}$, and refer to Martinec (2000) for parameterization of other field variables. For a fixed time, $\phi^E$ and $\boldsymbol{u}$ depending on co-latitude and longitude, $\Omega = (\theta, \varphi)$, are expanded in a series of scalar and vector spherical harmonics, respectively:

$$\begin{aligned} \phi^{\mathrm{E}}(r,\Omega) &= \sum_{j=0}^{\infty} \sum_{m=-j}^{m=j} F_{jm}(r)\, Y_{jm}(\Omega) \;, \\ \boldsymbol{u}(r,\Omega) &= \sum_{j=0}^{\infty} \sum_{m=-j}^{m=j} \left[ U_{jm}(r)\, \boldsymbol{S}^{(-1)}_{jm}(\Omega) \,+\, V_{jm}(r)\, \boldsymbol{S}^{(1)}_{jm}(\Omega) \,+\, W_{jm}(r)\, \boldsymbol{S}^{(0)}_{jm}(\Omega) \right] \;, \end{aligned} \tag{1}$$

where $0 \le r \le a$ with $a$ the radius of the Earth and $r$ the radial distance. The quantities $[F, U, V, W]_{jm}$ represent the spectral components, and $Y_{jm}$ and $\boldsymbol{S}^{(\lambda)}_{jm}$ are the respective scalar and vector spherical harmonics, see App. A. The summations spread over the angular degree $j$ and azimuthal order $m$. The potential is defined according to

$$\nabla^2 \phi^{\mathrm{E}} \,+\, 4\,\pi\, G\, \mathrm{div}(\rho_0 \boldsymbol{u}) \,=\, 0\;. \tag{2}$$

The representation of $\phi^{\mathrm{E}}$ and $\boldsymbol{u}$ in fully normalised spherical harmonics enables easy derivation of the equations for GC motion by applying the formalisms outlined in the theory of angular momentum (Varshalovich *et al.*, 1988). We solve the field equations directly in the time domain and do not apply any Love-number approach.

The degree-1 terms of the surface displacement, $U_{1m}$ and $V_{1m}$, describe net translations relative to the considered reference system. Among them, the center-of-figure (CF) motion is of most interest which describes the integral motion of the surface, as if it would be equally covered by an infinite dense array of points (Blewitt, 2003). In contrast, the degree-1 term of the surface displacement, $W_{1m}$, describes a surface net rotation and is set to zero as one uniqueness condition. The center-of-mass (CM) motion is defined by the first moment of the mass redistribution of the whole Earth (Blewitt, 2003). The difference between CF and CM motions, the geocenter (GC) motion, is of special interest due to its invariance with respect to the chosen reference frame.

## 2.1 Center-of-figure motion

In the dynamic modelling of the motions due a surface loading, we define a reference-state configuration of the Earth and define a reference system describing the position of mass points in this configuration. Here, the reference state describes the equilibrium state of a hydrostatically prestressed Earth where the reference system coincides with the reference configuration. Therefore, CF and CM coincide with the origin of the reference system. The variation of CF with respect to the origin of the reference system is defined by the net displacement of the surface. Considering (Eq. 1), this results in

$$\begin{aligned}\boldsymbol{u}_{\mathrm{cf}} &:= \frac{1}{A}\int_{\partial V}\boldsymbol{u}\,dS\\ &= \frac{1}{4\,\pi}\int_{\Omega_0}\sum_{jm}\left[U_{jm}\,\boldsymbol{S}_{jm}^{(-1)}+V_{jm}\,\boldsymbol{S}_{jm}^{(1)}+W_{jm}\,\boldsymbol{S}_{jm}^{(0)}\right]d\Omega\,,\end{aligned}\tag{3}$$

where $\partial V$ is the surface of the Earth and $\Omega_0 = 4\,\pi$ is the full solid angle.

Solving the integral, the Cartesian components of this motion are

$$
\begin{aligned}
u^x_{\mathrm{cf}} &= -\frac{1}{2}\sqrt{\frac{2}{3\,\pi}}\ \mathrm{Re}\{U_{11} + 2\,V_{11}\}\ , \\
u^y_{\mathrm{cf}} &= \frac{1}{2}\sqrt{\frac{2}{3\,\pi}}\ \mathrm{Im}\{U_{11} + 2\,V_{11}\}\ , \\
u^z_{\mathrm{cf}} &= \frac{1}{2}\sqrt{\frac{1}{3\,\pi}}(U_{10} + 2\,V_{10})\ ,
\end{aligned}
\tag{4}
$$

where $\boldsymbol{e}_x$, $\boldsymbol{e}_y$ and $\boldsymbol{e}_z$ are the Cartesian base vectors (see App. A). Here, one has to bear in mind that only these linear combinations describe a surface displacement, whereas the remaining parts, $\boldsymbol{u}(U_{1\,m}, V_{1\,m}) - \boldsymbol{u}_{\mathrm{cf}}$, describe a deformation.

## 2.2 Center-of-mass motion

The CM motion represents the motion of the first moment. Due to MacCullagh theorem (Munk & Macdonald, 1960), we define it here as the translation necessary to achieve the configuration where the degree-1 components of the gravitational potential, $\phi^{\mathrm{E}}$ in (Eq. 1) vanish. Representing the displacement vector of the center of mass, $\boldsymbol{u}_{\mathrm{cm}}$, in Cartesian coordinates, we obtain as outlined in App. B.1

$$
\begin{aligned}
u^x_{\mathrm{cm}} &= \frac{3}{2\,g_0}\sqrt{\frac{2}{3\,\pi}}\ \mathrm{Re}\{F_{11}\} = \frac{1}{g_0}\sqrt{\frac{3}{2\,\pi}}\ \mathrm{Re}\{F_{11}\} \\
u^y_{\mathrm{cm}} &= -\frac{3}{2\,g_0}\sqrt{\frac{2}{3\,\pi}}\ \mathrm{Im}\{F_{11}\} = -\frac{1}{g_0}\sqrt{\frac{3}{2\,\pi}}\ \mathrm{Im}\{F_{11}\} \\
u^z_{\mathrm{cm}} &= -\frac{3}{2\,g_0}\sqrt{\frac{1}{3\,\pi}}F_{10} = -\frac{1}{2\,g_0}\sqrt{\frac{3}{\pi}}\ F_{10}
\end{aligned}
\tag{5}
$$

where $g_0$ is the surface gravity and $F_{1m}$ are the degree-1 components of the potential increment $\phi^{\mathrm{E}}$ due to internal- and surface-mass redistribution.

## 2.3 Geocenter motion

The difference of CF amd CM motions define the GC motion

$$
\boldsymbol{u}_{\mathrm{gc}} = \boldsymbol{u}_{\mathrm{cf}} - \boldsymbol{u}_{\mathrm{cm}}\ ,
\tag{6}
$$

which is invariant to the chosen reference system according to the assumption made at the beginning of Sec. 2.1. By considering Eq.s 4 and 5, the Cartesian components of GC motion are

$$
\begin{aligned}
u^x_{\mathrm{gc}} &= -\frac{1}{2}\sqrt{\frac{2}{3\,\pi}}\,\mathrm{Re}\{\,U_{11} + 2\,V_{11} \,+\, 3\,F_{11}/g_0\,\}\ , \\
u^y_{\mathrm{gc}} &= \frac{1}{2}\sqrt{\frac{2}{3\,\pi}}\,\mathrm{Im}\{\,U_{11} + 2\,V_{11} \,+\, 3\,F_{11}/g_0\,\}\ , \\
u^z_{\mathrm{gc}} &= \frac{1}{2}\sqrt{\frac{1}{3\,\pi}}(\,U_{10} + 2\,V_{10} \,+\, 3\,F_{10}/g_0\,)\ .
\end{aligned}
\tag{7}
$$

Figure 1 shows the pattern of GC motion induced by GIA. The horizontal motion is directed towards Hudson Bay, the region of maximum glaciation during the last glacial cycle, causing the largest horizontal motion in the equatorial region wich is directed to the north. The vertical component is directed upward in the north and downward in the south. Fig. 1

# 3 Realizations of uniquenss condition

The field equations describing GIA induced deformations require specific uniqueness conditions (Martinec, 2000). We thus have a certain degree of freedom for choosing these conditions. In the following we discuss some possible uniqueness conditions on translation which we call realization of GIA-induced deformation.

## 3.1 Center-of-mass realization

In this realization, we assume that the CM is fixed to the reference system for all time steps. This means, all motions determined are expressed relative to CM. Considering in addition to the volumetric density, $\rho$, the surface-mass load change, $\sigma$, the first moment which we require to vanish consists of two parts:

$$
\boldsymbol{M}_\sigma + \boldsymbol{M}_\rho = \int_{\partial V} \sigma\,\boldsymbol{r}\,dS + \int_V \rho\,\boldsymbol{u}\,dV = 0\ . \tag{8}
$$

In this approximation, $\sigma(\boldsymbol{r}+\boldsymbol{u}) \simeq \sigma\,\boldsymbol{r}$ is assumed, which means that the displacement of the surface mass is not considered in $\boldsymbol{M}_\sigma$. This is acceptable because the displacement is rather small in comparison to the Earth's radius.

Considering material incompressibility, this integral can be represented by the spectral components of displacement and the spectral components of the load, $\Sigma_{1m}$, for degree 1:

$$\sqrt{\frac{4\pi}{3}}\, a^3\, \Sigma_{1m} \;+\; \sqrt{\frac{4\pi}{3}} \int_R \rho(r)\, r^2\, \left[ U_{1m}(r) \,+\, 2\, V_{1m}(r) \right] \, dr \;=\; 0\,, \tag{9}$$

where $\rho(r)$ is the density distribution in the reference state and the integral covers the Earth's interior.

## 3.2 Center-of-figure realization

In this realization, the integral over the surface displacement has to vanish:

$$\int_{\partial V} \boldsymbol{u}\, dS \;=\; 0 \tag{10}$$

Solving this integral, the condition is fullfilled if

$$U_{1m}(a) \,+\, 2\, V_{1m}(a) \;=\; 0 \tag{11}$$

for all time steps.

## 3.3 Center-of-deformation realization

A further uniqueness condition is realised if only mass transport inside the Earth's body is considered, which is called the center of internal Earth, CE (Blewitt, 2003). Here, the integral over the mass displacement inside the Earth has to vanish. This means, only $\boldsymbol{M}_\rho$ in (Eq. 8) is considered to vanish,

$$\boldsymbol{M}_\rho \;=\; \int_V \rho\, \boldsymbol{u}\, dV \;=\; 0\,, \tag{12}$$

which results in

$$\sqrt{\frac{4\pi}{3}} \int_R \rho(r)\, r^2\, \left[ U_{1m}(r) \,+\, 2\, V_{1m}(r) \right] \, dr \;=\; 0\,. \tag{13}$$

In this case, the CM and the CF motions do not vanish.

Figure 2 shows $\boldsymbol{u}_{\mathrm{cf}}$, $\boldsymbol{u}_{\mathrm{cm}}$ and $\boldsymbol{u}_{\mathrm{gc}}$ for the CE realization during the whole last glacial cycle. We considered the LM+ model, which consists of a low viscous upper mantle, $\eta_{\mathrm{UM}} = 5 \times 10^{20}$ Pa s, and a high viscous lower mantle, $\eta_{\mathrm{LM}} = 1 \times 10^{22}$ Pa s. The advantage of this realization is, that we are able to distinguish between the contribution of surface-mass changes, which are represented by the CM motion and that due to the change of the Earth's shape represented by the CF motion. It becomes evident that, after deglaciation, the component of CM is rather small which was already discussed by Argus (2007). The contributions to the present time velocity of the GC motion are presented in Tab. 1 and show that the oceanic water redistribution following the GIA-induced changing geoid contributes less than 0.05 mm/yr (2nd row in table). Its direction points towards the north Atlantic for the considered model. The predicted GC motion at present day is of the order of 1 mm/yr and, therefore, should be considered in kinematics of the Earth's surface.

Fig. 2

Tab. 1

### 3.4 Invariance of geocenter motion

The geocenter (GC) motion is a relative motion which is invariant against a coordinate transformation. This invariance is proofed numerically by running the same loading scenario in the different realizations. We analyse the difference between the surface velocity field in the CM and CF realization considering the same loading scenario. The velocity field

$$\boldsymbol{u}_{\mathrm{gc}}(\boldsymbol{\Omega}) = \boldsymbol{u}^{\mathrm{CM}}(\boldsymbol{\Omega}) - \boldsymbol{u}^{\mathrm{CF}}(\boldsymbol{\Omega}) \tag{14}$$

describes the geocenter motion. Here, $\boldsymbol{u}^{\mathrm{CM}}$ is the surface velocity field determined in the CM realization and $\boldsymbol{u}^{\mathrm{CF}}$ is the surface velocity field determined in the CF realization by applying (Eq. 1), respectively. This motion should be the same as the motion defined by applying (Eq. 7) in any realization. Fig. 3 shows the differences which are, as expected, negligible with respect to the motion itself.

Fig. 3

### 3.5 Liquid-core approximation

In an often considered approximation, the solution domain is restricted to the viscoelastic lithosphere and mantle, and the core is considered as an inviscid sphere with a uniform density, determined such that it gives the same gravity as the real Earth's core.

According to Tromp & Mitrovica (1999), the interaction between core and mantle results in a specified relation between the gravity potential at the core–mantle boundary (CMB) and the pressure perturbation due to the normal displacement of the CMB. Then, the solution domain, $V$, can be restricted to the Earth's crust and mantle, and the influence of the core is considered as boundary condition.

To consider this approximation in the CM realization, (Eq. 8) is replaced by the respective first moments of the surface mass, the mass displacements inside $V$ and the first moment of the liquid core:

$$\boldsymbol{M}_\sigma + \boldsymbol{M}_\rho + \boldsymbol{M}_{\mathrm{lq}} = 0 \qquad (15)$$

The first moment of the liquid core motion is according to App. B.2

$$\boldsymbol{M}_{lq} = \sqrt{\frac{4\,\pi}{3}}\, r_C^3\, \bar{\rho}_C \sum_{m=-1}^{+1} U_{1\,m}(r_C{}^+)\, \boldsymbol{e}_m\ , \qquad (16)$$

where $r_C$ is the core radius, $\bar{\rho}_C$ is the average core density, $U_{1\,m}(r_C{}^+)$ are the displacements above the CMB and $\boldsymbol{e}_m$ are the spherical contravariant base vectors.

In order to keep the reference gravity at the surface, $\bar{\rho}_C$ has to be the volume average of the density stratification inside the core. This means that the buoyancy force at the CMB, which is determined from $[\bar{\rho}_C - \rho(r_C{}^+)]\,(\boldsymbol{u}^+ \cdot \boldsymbol{e}_r)$, is systematically increased by 20 %, if we compare $\bar{\rho}_C = 10952$ kg m$^{-3}$, the density below the CMB inferred from PREM, $\rho(r_C{}^-) = 9903$ kg m$^{-3}$, and that above the CMB, $\rho(r_C{}^+) = 5550$ kg m$^{-3}$.

The consequences for GIA should be small, but a systematic deviation can be expected. We analysed the effect on the displacement rates and gravity change at present day by comparing a model with viscoelastic core structure, VVE, with a model where the core is included as a liquid-core boundary condition, VLQ. For VVE, we considered a standard viscosity stratification LM+, the ICE-5G glaciation history and, for the viscoelastic core, the PREM density structure. For numerical reasons, we cannot model a purely Newtonian fluid and assume the outer-core shear modulus to be the same as the inner-core shear modulus, $\mu_{\rm OC} = 7.036 \times 10^{10}$ N/m$^2$. Based on the analysis of the free-core nutation, the inner-core viscosity lies in between $10^{12}$ and $10^{17}$ Pa s Greff-Lefftz *et al.* (2000). Again for numerical reasons and for our main interest in the influence of the density contrast at the CMB, we assume the viscosity in the whole core to be constant with $\eta_{\rm C} = 5 \times 10^{19}$ Pa s. The resulting Maxwell time, $\eta_{\rm OC}/\mu_{\rm OC} = 22$ yr, is rather small and we expect the deviation from an inviscid fluid to be negligible.

Figure 4 shows the relative deviation between a model assuming a viscoelastic stratified core and a model assuming a homogeneous fluid core, where the effect on vertical, horizontal and gravity displacement rates at present time are plotted as function of degree and order. The considered realization of these models is the CF system. The relative difference is calculated according to

$$\delta = \frac{|A_{jm} - B_{jm}|}{\frac{1}{2}|A_{jm} + B_{jm}|} \ , \tag{17}$$

where $A_{jm}$, $B_{jm}$ are the respective spectral amplitudes of the two models. Fig. 4

For low degrees, the largest deviation of almost 5 % in the vertical displacement rate appears at the term $(j, m) = (3, 0)$. In contrast, the horizontal displacement rate shows its largest deviation at the term $(4, 3)$. For higher degrees, the deviation is about 0.2 to 0.6 % with further peaks of more than 1 % deviation at the terms $(6, 6)$ and $(9, 7)$. The differences at degree 1 are about 3 to 4 %.

In a further run, we verify that a low-viscous core mimics the behaviour of a fluid core. We assume a viscoelastic homogeneous core with $\eta_{\rm C} = 5 \times 10^{19}$ Pa s and the average density of $\bar{\rho}_C$ and compare the present day spectral rates with those of the model run with a fluid core approximation. The analysis presented in Fig. 5 shows that the fluid core approximation accounts for an error of Fig. 5

less then 1 % for all spectral degrees and surface components.

This enables us to use Fig. 4 to determine the accuracy if a fluid core approximation, where a homogeneous core density has to be assumed, replaces a realistically stratified core. The error of the GIA induced geocenter motion determined with a fluid core approximation is less than 5 %.

## 4 Influence of mantle viscosity

Now, the influence of material parameters in the Earth's interior on the induced geocenter motion is discussed. We concentrate on the upper- and lower-mantle viscosity as well as the lithosphere thickness and vary one parameter at a time keeping the others constant at the reference values of 90 km thick lithosphere, $5 \times 10^{20}$ Pa s upper-mantle viscosity and $1 \times 10^{22}$ Pa s lower-mantle viscosity (e.g. Wolf *et al.*, 2006). The loading model ICE-5G is considered unchanged for all the model runs. Fig. 6

In the first experiment, we vary the lower-mantle viscosity between $5 \times 10^{19}$ Pa s and $10^{25}$ Pa s. This range is much wider than the expected average viscosity of the lower mantle wich varies between $10^{21}$ Pa s and $10^{23}$ Pa s (e.g. Steinberger & Holme, 2008). The consideration of a broader range of lower-mantle viscosity enables a better discussion of the physical behaviour. Fig. 6a shows the variation of the geocenter motion with lower-mantle viscosity, where, on the left, the geographical position of the direction of the velocity vector is plotted and, on the right, the absolute rate as a function of lower mantle viscosity. At $10^{21}$ Pa s, we find a minimum value of about 0.1 mm/yr. A maximum value of 0.9 mm/yr is reached at $10^{22}$ Pa s. If the lower-mantle viscosity is further increased, the velocity reduces and reaches an asymptotic value of 0.5 mm/yr for viscosities larger than $10^{23}$ Pa s. This asymptote is placed at the geographical point 65 °N/72 °W. For these values of lower-mantle viscosities, the total viscous flow is confined to the upper mantle and the lower mantle behaves like an elastic continuum. In contrast to the strongly varying amplitude of the velocity vector by almost one order in magnitude, which was already discussed by Greff-Lefftz

(2000), the direction is rather stable and varies by 2000 km. Only for unrealistically small viscosity values of less then $10^{20}$ Pa s, the direction changes drastically. Here, we found a turning of the direction to the southern hemisphere (not shown).

The influence of upper mantle viscosity is discussed in the second numerical experiment shown in Fig. 6b, where the upper-mantle viscosity varies between $10^{20}$ Pa s and $10^{22}$ Pa s. As a result, the influence is smaller than for the lower-mantle viscosity. Again, we find a first minimum at $2 \times 10^{20}$ Pa s at 0.6 mm/yr and a maximum at $6 \times 10^{20}$ Pa s which resembles the reference value. For higher viscosities, we observe a linear reduction with the logarithm of the viscosity, where at $10^{22}$ Pa s a value of 0.5 mm/yr is reached. Concerning the direction variations of the velocity, we find a much smaller variability than for the lower-mantle viscosity at 65 $^{\circ}$N/69 $^{\circ}$W. With increasing upper-mantle viscosity, we observe a slight movement of the velocity vector to the East.

The smallest influence on the position and magnitude of the velocity shows the lithosphere thickness (Fig. 6c) where almost no variation of the direction is observable. The absolute velocity decreases linearly from 1.05 mm/yr at 50 km thickness to 0.75 mm/yr at 130 km thickness.

Summarising, we find, that due to the long spatial wavelength of the degree-1 deformation, the influence of lower-mantle viscosity is largest, whereas the upper-mantle viscosity and lithosphere thickness are only of minor influence on the velocity magnitude of the geocenter motion, and the influence on the direction of the velocity is negligible. Likewise, lower-mantle viscosity larger than $10^{23}$ Pa s shows a strong influence on the magnitude of velocity, but only moderate effect on its direction.

## 5 Influence of glaciation history

A further factor influencing the glacially induced geocenter motion is the history of the three main ice sheets during the Pleistocene glaciations, which are Laurentide, Fennoscandia and Antarctica. We use the reference visosity model, LM+, discussed in the previous section. The glaciation history ICE-5G will be rescaled by different weighting of the individual areas of glaciation.

We perform two tests. First, we keep the total mass of ice constant, but vary the mass of one of the main areas, Laurentia, Fennoscandia and Antarctica, between fraction $x = 0.85$ and 1.15 in steps of 5 %. To do this, the load thicknesses are multiplied pointwise with $x$, and the thicknesses of all other areas are multiplied by $y$, chosen such that the total ice mass is conserved:

$$\begin{aligned} M_{\mathrm{Laur}} + M_{\mathrm{rest}} &= M_{\mathrm{total}} , \\ M'_{\mathrm{Laur}} &= x\, M_{\mathrm{Laur}} , \\ \Rightarrow \quad y &= \frac{M_{\mathrm{total}} - x\, M_{\mathrm{Laur}}}{M_{\mathrm{rest}}} . \end{aligned} \tag{18}$$

Figure 7a shows the geocenter motion for variations in ice mass of Laurentia, Fennoscandia and Antarctica which is rather stable located north of Hudson Strait. The influence of Laurentia is largest and varies between 0.75 and 1 mm/yr if the fraction, $x$, varies between 0.85 and 1.15. The influence of Fennoscandia is smaller and that of Antarctica is of opposite sign and of similar magnitude like Laurentia. The opposite sign is due to the location of the ice sheet on the southern hemisphere. Therefore, a larger rebound signal on the southern hemisphere reduces the geocenter velocity, whereas the vector direction is less influenced. Fig. 7

In a second experiment (Fig. 7b), the total mass of the ice is not conserved when varying the thicknesses of the individual areas of Pleistocene glaciation. But, the surface mass of ocean and ice remains conserved by applying the sea-level equation in all calculations (e.g. Farrell & Clark, 1976). Here, the direction varies much less for varying $x$ of Laurentide due to the fact, that the mass loss or gain of this dominating ice sheet is not distributed to the remaining ice sheets.

In order to investigate the sensitivity to the considered glaciation history we replace the Antarctic glaciation part in in ICE-5G by the glaciation history IJ05 (Ivins & James, 2005). To discuss this feature, we also increase the range of load fraction for ICE-5G Antarctica from 0.5 to 2. For the IJ05 scenario, we get a geocenter motion shifted 10 $^{\circ}$S with a velocity of 0.75 mm/yr as indicated by the yellow diamond in Fig. 7b. This value is similar to the scenario, where the load fraction of Antarctica is increased by a factor of 1.5 or for the direction an increase of the load by a factor of 2. This result is contradicting, because the maximum mass of IJ05 is by a factor of 2 smaller than the mass of ICE-5G. Considering the history of deglaciation (Fig. 8), it becomes evident, that the uplift signal due to IJ05 is more pronounced because the melting terminated much later in history and so, at present time the relaxation process is much stronger than for ICE-5G. So, the influence of the loading history is of same importance as that of the viscosity structure. Fig. 8

Repeating this study with the viscosity model VM2, which shows an average viscosity in the lower mantle of $2 \times 10^{21}$ Pa s, we find a similar variability like for viscosity model LM+ (Fig. 9). The pattern are similar, but the absolute velocity is reduced to 0.2 mm/yr and the velocity direction is shifted to the south as exptected from Fig. 6a. Fig. 9

## 6 Conclusion

We discussed the influence of Earth and loading parameters for the glacially induced geocenter motion which is defined in accordance with Blewitt (2003) as the motion of the center of figure relative to the center of mass. We revisited the theoretical background, which we had to reformulate slightly for the solution method adopted and varified numerically the invariance of the geocenter motion with respect to the chosen uniqueness conditions in our numerical formulation. The consideration of the fluid-core as a boundary condition resulting from the static approximation was checked to be exceptable for the degree-1 component in the solutions showing a systematic deviation of less than 5 %.

The second focus was to assess the variability of the geocenter motion with respect to Earth-model parameters. We showed that the lower-mantle viscosity has the strongest influence resulting in a variation of the velocity amplitude of almost one order in magnitude which confirms the results of Greff-Lefftz (2000). The influence of the upper-mantle viscosity and lithosphere thickness was comparable small. For all parameterizations, we found a rather robust direction of the GIA-induced geocenter motion pointing towards east of Hudson Bay.

The assumption that the glaciation history is of similar importance was investigated. We found that by only weighting the areas of glaciation differently, the variability of the velocity is moderate and largest for the Laurentide ice sheet.

A much stronger influence was found when changing the time evolution of the deglaciation. We showed that for the glaciation history IJ05 for Antarctica, the geocenter motion is larger than due to the Antarctic part of ICE-5G, because the former model shows later deglaciation, and thus a stronger GIA signal at present time although its mass at last glacial maximum is half of that for ICE-5G.

# Acknowledgments

We thank for the constructive remarks of two anonymous reviewers which guided us to consider the inner-core viscosity. The research of the work of the first author is funded by the Deutsche Forschungsgemeinschaft (DFG, German Research Foundation) through research grant MA3432/2-2 (SPP1257). The second author acknowledges support from the Grant Agency of the Czech Republic through Grant No. 205/09/0546. The Generic Mapping Tools, GMT, (Wessel & Smith, 1991) were employed for preparation of the figures.

# References

Argus, D. F., 2007. Defining the translational velocity of the reference frame of Earth. *Geophys. J. Int.*, 169: 830–838.

Blewitt, G., 2003. Self-consistency in reference frames, geocenter definition, and surface loading of the solid earth. *J. Geophys. Res.*, 108: 2103.

Blewitt, G., Lavallée, D., Clarke, P. & Nurutdinov, K., 2001. A new global mode of earth deformation: Seasonal cycle detected. *Science*, 294: 2342–2345.

Bouillé, F., Cazenave, A., Lemoine, J. & Cretaux, J., 2000. Geocenter motion from the DORIS space system and laser data on Lageos satellites: comparison with surface loading data. *Geophys. J. Int.*, 143: 71–82.

Chen, J., Wilson, C., Eanes, R. & Nerem, R., 1999. Geophysical interpretation of observed geocenter variations. *J. Geophys. Res.*, 104: 2683–2690.

Crossley, D. J. & Gubbins, D., 1975. Static deformations of the Earth's liquid core. *Geophys. Res. Lett.*, 2: 1–4.

Dong, D., Yunck, T. & Heflin, M., 2003. Origin of the international Terrestrial Reference Frame. *J. Geophys. Res.*, 108: 2200.

Farrell, W. E. & Clark, J. A., 1976. On postglacial sea level. *Geophys. J. R. Astr. Soc.*, 46: 647–667.

Greff-Lefftz, M., 2000. Secular variation of the geocenter. *J. Geophys. Res.*, 105: 25685–25692.

Greff-Lefftz, M., Legros, H. & Dehant, V., 2000. Influence of the inner core viscosity on the rotational eigenmodes of the Earth. *Phys. Earth Planet. Inter.*, 122: 187–204.

Heflin, M., Bertiger, W., Blewitt, G., Freedman, A., Hurst, K., Lichten, S., Lindqwister, U., Vigue, Y., Webb, F., Yunck, T. & Zumberge, J., 1992. Global geodesy using GPS without fiducial sites. *Geophys. Res. Lett.*, 19: 131–134.

Heiskanen, W. A. & Moritz, H., 1967. *Physical Geodesy*. W. H. Freeman and C., London.

Ivins, E. R. & James, T. S., 2005. Antarctic glacial isostatic adjustment: a new assessment. *Antarct. Sci.*, 17: 537–549.

Kang, Z., Tapley, B., Chen, J., Ries, J. & Bettadpur, S., 2009. Geocenter variations derived from GPS tracking of the GRACE satellites. *Journal of Geodesy*, pp. 7–+.

Kreemer, C., Lavallee, D. A., Blewitt, G. & Holt, W. E., 2006. On the stability of a geodetic no-net-rotation frame and its implication for the International Terrestrial Reference Frame. *Geophys. Res. Lett.*, 33: L17306.

Lavallée, D. A., van Dam, T., Blewitt, G. & Clarke, P. J., 2006. Geocenter motions from GPS: A unified observation model. *J. Geophys. Res.*, 111: B05405, doi:10.1029/2005JB003784.

Martinec, Z., 1999. Spectral, initial value approach for viscoelastic relaxation of a spherical earth with a three-dimensional viscosity—I. Theory. *Geophys. J. Int.*, 137: 469–488.

Martinec, Z., 2000. Spectral–finite element approach for three-dimensional viscoelastic relaxation in a spherical earth. *Geophys. J. Int.*, 142: 117–141.

Martinec, Z. & Hagedoorn, J., 2005. Time-domain approach to linearized rotational response of a three-dimensional viscoelastic earth model induced by glacial-isostatic adjustment: I. inertia-tensor perturbations. *Geophys. J. Int.*, 163: 443–462.

Munk, W. H. & Macdonald, G. J. F., 1960. *The Rotation of the Earth - A Geophysical Discussion*. Cambridge University Press.

Pěč, K. & Martinec, Z., 1982. Expansion of geoid heights into spherical harmonic series. *Stud. Geophys. Geod.*, 26: 115–119.

Peltier, W. R., 1974. The impulse response of a Maxwell earth. *Rev. Geophys. Space Phys.*, 12: 649–669.

Peltier, W. R., 2004. Global glacial isostasy and the surface of the ice-age earth: the ICE5G (VM2) model and GRACE. *Ann. Rev. Earth Planet. Sci.*, 32: 111–149.

Steinberger, B. & Holme, R., 2008. Mantle flow models with core-mantle boundary constraints and chemical heterogeneities in the lowermost mantle. *J. Geophys. Res.*, 113: B05403, doi:10.1029/2007JB005080.

Tromp, J. & Mitrovica, J. X., 1999. Surface loading of a viscoelastic earth—I. general theory. *Geophys. J. Int.*, 137: 847–855.

Tushingham, A. M. & Peltier, W. R., 1991. ICE-3G: a new global model of the late Pleistocene deglaciation based upon geophysical predictions of post-glacial relative sea level change. *J. Geophys. Res.*, 96: 4497–4523.

Varshalovich, D. A., Moskalev, A. N. & Khersonskii, V. K., 1988. *Quantum Theory of Angular*

*Momentum*. World Scientific Publishing, Singapore.

Vermeersen, L. L. A., Sabadini, R., Devoti, R., Luceri, V., Rutigliano, P., Sciarretta, C. & Bianco, G., 1998. Mantle viscosity inferences from joint inversions of Pleistocene deglaciation-induced changes in geopotential with a new SLR analysis and polar wander. *Geophys. Res. Lett.*, 25: 42614264.

Wessel, P. & Smith, W. H. F., 1991. Free software helps map and display data. *EOS, Trans. Am. Geophys. Union*, 72: 441–446.

Wolf, D., Klemann, V., Wünsch, J. & Zhang, F.-p., 2006. A reanalysis and reinterpretation of geodetic and geomorphologic evidence of glacial-isostatic uplift in the Churchill region, Hudson Bay. *Surv. Geophys.*, 27: 19–61.

Wu, P. & Peltier, W. R., 1982. Viscous gravitational relaxation. *Geophys. J. R. Astr. Soc.*, 70: 435–485.

Wu, X., Heflin, M. B., Ivins, E. R. & Fukumori, I., 2006. Seasonal and interannual global surface mass variations from multisatellite geodetic data. *J. Geophys. Res.*, 111: B09401, doi:10.1029/2005JB004100.

Wu, X., Heflin, M., Schotman, H., Vermeersen, B., Dong, D., Gross, R., Ivins, E., Moore, A. & Owen, S., 2009. Global estimation of present-day surface mass trend and glacial isostatic adjustment. *Science*, submitted.

# A Generalization of spherical harmonics

Due to the weak formulation of glacial-isostatic adjustment in the theory of Martinec (1999), the spectral base functions follow the quantum mechanic norm, e.g. outlined in Varshalovich *et al.* (1988) [in the following abbreviated by Varsh. *Sect*. (*Eq.*)]. Their main features are the normalisation, (Varsh. 5.1.3 (6)),

$$\int_{\Omega_0} Y_{j\,m}\, Y_{k\,n}\, d\Omega \;=\; \delta_{jk}\, \delta_{mn} \;, \tag{19}$$

where $\delta_{jk}$ is the Kronecker-delta, and the Condon-Shortley phase, meaning that $Y_{j\,0}$ are real and, for the conjugate complex holds $Y^*_{j\,m}(\vartheta,\varphi) \;=\; Y_{j\,m}(\vartheta,-\varphi) \;=\; (-1)^m\, Y_{j\,-m}(\vartheta,\varphi)$ (Varsh. 5.1.3 (11)).

The transformation from complex coefficients, $A_{jm}$, for the representation of a scalar field in fully normalized spherical harmonics considered here, into real Stokes' coefficients, $C_{jm}$ and $S_{jm}$, widely used in geodesy (e.g. Heiskanen & Moritz, 1967), follows according to Pěč & Martinec (1982)

$$\begin{aligned}
A_{j\,0} \;&=\; \sqrt{4\,\pi}\, C_{j\,m} \;, \\
A_{j\,m} \;&=\; (-1)^m \sqrt{2\,\pi}\; [C_{j\,m} - i\, S_{j\,m}] \;, \qquad && m > 0 \;, \\
A_{j\,-m} \;&=\; (-1)^m A^*_{j\,m} \;, && m > 0 \;.
\end{aligned} \tag{20}$$

The generalization of the scalar spherical harmonics to their vector forms follows Martinec (2000, Eq. b3),

$$\begin{aligned}
\boldsymbol{S}^{(-1)}_{j\,m} \;&:=\; e_r\, Y_{j\,m} \;, \\
\boldsymbol{S}^{(+1)}_{j\,m} \;&:=\; \boldsymbol{\nabla}_\Omega Y_{j\,m} \;, \\
\boldsymbol{S}^{(0)}_{j\,m} \;&:=\; (\boldsymbol{e}_r \,\times\, \boldsymbol{\nabla}_\Omega) Y_{j\,m} \;,
\end{aligned} \tag{21}$$

which slightly differ from the definitions in Varsh. 7.3.1 (6). Conversion into the latter follows according to

$$\begin{aligned}
\boldsymbol{Y}^{(-1)}_{j\,m} &= \boldsymbol{S}^{(-1)}_{j\,m}\,, \\
\boldsymbol{Y}^{(+1)}_{j\,m} &= \frac{1}{\sqrt{j(j+1)}}\,\boldsymbol{S}^{(+1)}_{j\,m}\,, \\
\boldsymbol{Y}^{(0)}_{j\,m} &= \frac{-i}{\sqrt{j(j+1)}}\,\boldsymbol{S}^{(0)}_{j\,m}\,.
\end{aligned} \tag{22}$$

The advantage of (Eq. 21) is that all three vector spherical harmonics transform according to

$$\boldsymbol{S}^{(\mu)}_{j\,-m} = (-1)^m\,[\boldsymbol{S}^{(\mu)}_{j\,m}]^*\,, \quad \mu = -1,0,1\,, \tag{23}$$

and therefore the components, $F$, $U$, $V$, $W$, of (Eq. 1) in the same way.

The covariant base vectors, $\boldsymbol{e}_\mu$, $\mu = \{-1,0,1\}$, of these functions are defined like in Varsh. 1.1.3 (20), and the contravariant spherical coordinates, $x^\mu$, are transformed into Cartesian coordinates according to

$$\begin{aligned}
x &= \frac{1}{\sqrt{2}}\,(x^{-1} - x^{+1})\,, \\
y &= \frac{-i}{\sqrt{2}}\,(x^{-1} + x^{+1})\,, \\
z &= x^0\,.
\end{aligned} \tag{24}$$

# B Proofs

In this appendix some derivations are presented.

## B.1 Proof of Eq. 5

The CM motion describes the shift of the coordinate system such that the degree-1 component of the gravitational potential $\phi = \phi_0 + \phi_1$ vanishes in the shifted coordinate system. In other words, the center-of-mass coincides with the origin of the shifted coordinate system.

*Proof.* Representing the external gravitational potential by

$$\phi(r,\Omega) = \sum_{j\,m} F^{\mathrm{ext}}_{j\,m}\left(\frac{a}{r}\right)^{j+1} Y_{j\,m}(\Omega) \tag{25}$$

and considering the continuity of the potential at the Earth's surface,

$$F^{\text{ext}}_{j\,m} = F_{j\,m}(a^-)\,, \tag{26}$$

the potential in a shifted coordinate system described by a pure translation, $(d, \Omega_d)$, can be expressed by

$$\phi(r_2,\Omega_2) = \sum_{j\,m} F_{j\,m}(a^-)\,a^{j+1}\,\frac{1}{r_2^{j+1}}\,Y_{j\,m}(\Omega_2)\,, \tag{27}$$

where, Varsh. 5.17.6 (36),

$$\begin{aligned}\frac{1}{r_2^{j+1}}\,Y_{j\,m}(\Omega_2) &= \sqrt{\frac{4\,\pi}{(2\,j)!}}\sum_{\substack{j_1,j_2=0\\ j_1-j_2=j}}\sqrt{\frac{(2\,j_1)!}{(2\,j_2+1)!}}\,\frac{d^{j_2}}{r_1^{j_1+1}}\\ &\quad\times\sum_{m_1,m_2} C^{j\,m}_{j_1\,m_1\,j_2\,m_2}\,Y_{j_1\,m_1}(\Omega_1)\,Y_{j_2\,m_2}(\Omega_d)\,.\end{aligned} \tag{28}$$

$d$ is the amplitude of shift and $\Omega_d$ is the angle of shift. Rearranging Eq.s 27 and 28, we find

$$\phi(r_2,\Omega_2) = \sum_{j_1\,m_1} V_{j_1\,m_1}\,Y_{j_1\,m_1}(\Omega_1)\,, \tag{29}$$

where

$$V_{j_1\,m_1} = \sum_{j\,m} F_{j\,m}\,\frac{a^{j+1}}{r_2^{j_1+1}}\sqrt{\frac{4\,\pi}{(2\,j)!}}\sum_{\substack{j_2=0\\ j_2=j_1-j}}\sqrt{\frac{(2\,j_1)!}{(2\,j_2+1)!}}\,d^{j_2}\sum_{m_2} C^{j\,m}_{j_1\,m_1\,j_2\,m_2}\,Y_{j_2\,m_2}(\Omega_d)\,. \tag{30}$$

The CM motion is determined by vanishing $V_{1\,m_1}$. Since $j_1 = 1$ and $j_2$ is non-negative, $j$ equals 0 or 1. Hence

$$\begin{aligned}V_{1\,m_1} &= \sum_{j\,m} F_{jm}\,a^{j-1}\sqrt{\frac{4\,\pi}{(2\,j)!}}\sum_{\substack{j_2=0\\ j_2=1-j}}\sqrt{\frac{2!}{(2\,j_2+1)!}}\,d^{j_2}\sum_{m_2} C^{j\,m}_{j_1\,m_1\,1-j\,m_2}\,Y_{j_2\,m_2}(\Omega_d)\\ &= F_{00}\frac{1}{a}\sqrt{4\,\pi}\sqrt{\frac{2!}{3!}}\,d^1\sum_{m_2} C^{0\,0}_{1\,m_1\,1\,m_2}\,Y_{1\,m_2}(\Omega_d)\\ &\quad+\sum_m F_{1\,m}\sqrt{\frac{4\,\pi}{1!}}\sqrt{\frac{2!}{1!}}\,C^{1\,m}_{1\,m_1\,0\,0}\,Y_{0\,0}(\Omega_d)\\ &= F_{00}\frac{d}{a}\frac{\sqrt{4\,\pi}}{3}\,(-1)^{m_1+1}\,Y_{1\,-m_1}(\Omega_d) + F_{1\,m_1}\,.\end{aligned}$$

(31)

In the last expression, we replaced the Clebsch–Gordan coefficients

$$C^{0\,0}_{1\,m_1\,1\,m_2} = (-1)^{m_1+1}\,\frac{\delta_{m_1\,-m_2}}{\sqrt{3}} \qquad \text{(Varsh. 8.5.1 (1))}, \tag{32}$$

$$C^{1\,m}_{1\,m_1\,0\,0} = \delta_{m_1\,m} \qquad \text{(Varsh. 8.5.1 (2))}, \tag{33}$$

and $Y_{0\,0} = 1/\sqrt{4\,\pi}$. In view of Eqs. 31 and the reference potential of the Earth, $F_{00} = \sqrt{4\,\pi}\,g_0\,a$, the condition $V_{1m_1} = 0$ reads as

$$\frac{F_{1\,m_1}}{g_0} = \frac{4\,\pi}{3}\,d\,(-1)^{m_1} Y_{1\,-m_1}(\Omega_d)\;, \tag{34}$$

where $m_1 = +1, 0, -1$. Moreover considering the explicit forms of $Y_{1\,m}$, Varsh. 5.13.1 (2), the contravariant spherical coordinates, Varsh. 1.1.3 (18), of the CM motion have the form

$$\begin{aligned} u^{+1}_{\text{cm}} &= -\sqrt{\frac{1}{2}}\,d\,\sin\theta\,e^{-i\phi} = \frac{1}{2}\sqrt{\frac{3}{\pi}}\,\frac{F_{1\,-1}}{g_0}\;, \\ u^{0}_{\text{cm}} &= d\,\cos\theta = \frac{1}{2}\sqrt{\frac{3}{\pi}}\,\frac{F_{10}}{g_0}\;, \\ u^{-1}_{\text{cm}} &= \sqrt{\frac{1}{2}}\,d\,\sin\theta\,e^{i\phi} = \frac{1}{2}\sqrt{\frac{3}{\pi}}\,\frac{F_{1\,1}}{g_0}\;, \end{aligned} \tag{35}$$

where the second equalities follow from the condition (Eq. 34). With $F_{1\,-1} = -F^*_{1\,1}$ and the relation between the Cartesian and contravariant spherical coordinates (Eq. 24), the expressions (Eq. 5) are obtained.

□

## B.2 Proof of Eq. 16

The derivation for the first moment of a deformable, incompressible and homogeneous fluid follows Martinec & Hagedoorn (2005):

*Proof.* The first moment of the core is considered in the Eulerian domain and is split into the integral over the reference volume and the additional part due to the undulation of the CMB:

$$\boldsymbol{M}_{lq} = \int_{V^0} \rho^E(t)\,\boldsymbol{r}\,dV + \int_{V(t)-V^0} \rho^E(t)\,\boldsymbol{r}\,dV \tag{36}$$

The second integral is approximated by a surface integral, $\int_{V(t)-V^0} dV = \int_{\partial V^0} (\boldsymbol{n}^0 \cdot \boldsymbol{u})\, dS$, which is correct in first order of $||\boldsymbol{n}^0 \cdot \boldsymbol{u}||$. Considering material incompressibility, $\rho^E(t) = \rho_C$, $\boldsymbol{n}^0 = \boldsymbol{e}_r$ and $V^0 = V^C$ we get

$$\boldsymbol{M}_{lq} = \int_{V^C} \rho_C\, \boldsymbol{r}\, dV + \int_{\partial V^C} \rho_C\, (\boldsymbol{e}_r \cdot \boldsymbol{u})\, \boldsymbol{r}\, dS \,. \tag{37}$$

The first term describes the momentum in the reference state and is zero for a homogeneous fluid. In the second term, we identify

$$(\boldsymbol{e}_r \cdot \boldsymbol{u})\, \boldsymbol{r} = r \sum_{jm} U_{j\,m}\, \boldsymbol{S}^{(-1)}_{j\,m} \,, \tag{38}$$

consider $dS = r_C^2\, d\Omega$ and apply the solution of $\int_{\Omega_0} \boldsymbol{S}^{(-1)}_{j\,m}\, d\Omega$, Varsh. 7.3.12 (118), in order to achieve Eq. 16. $\square$

| Model | Cartesian comp. (mm/yr) | | | Geogr. components | | |
|---|---|---|---|---|---|---|
| | $u_x$ | $u_y$ | $u_z$ | Lon. (°E) | Lat. (°N) | $\|\dot{\boldsymbol{u}}\|$ (mm/yr) |
| CF | 0.157472 | -0.346818 | 0.840379 | -65.5797 | 65.618 | 0.922668 |
| CM | 0.0242489 | -0.0121181 | 0.0346408 | -26.5531 | 51.9549 | 0.0439868 |
| GC | 0.133173 | -0.334511 | 0.805666 | -68.2919 | 65.9205 | 0.882457 |

Table 1: Present day center-of-figure (CF) velocity, center-of-mass (CM) velocity and geocenter (GC) velocity in the CE realization.

Figure 1: Surface-displacement velocities due to a center-of-figure motion of 0.8 mm/yr towards Hudson Bay.

Figure 2: Evolution of geocenter, center-of-figure and center-of-mass motion in the CE realization as function of time before present (BP).

Figure 3: Difference in determining the geocenter motion using the velocity fields in the two realizations by applying Eq. 14, and calcuating directly from degree 1 by applying Eq. 7. In left panel, colors indicate the vertical component and, in right panel, colors indicate the horizontal amplitude. The maximum deviation is $-0.0013$ mm/yr in the vertical velocity and $0.0002$ mm/yr in the horizontal amplitude.

Figure 4: Relative difference, $\delta$, of rates in vertical (black), horizontal (red), potential (blue) amplitude between model VVE and model VLQ. Abscissa is multi-index of $(j, m)$. Associated Legendre coefficients are denoted by numbers and vertical lines: The numbers from 1 to 10 denote the respective Legendre degree, $j$. The order increases from $m = 0$ to $j$ starting at the vertical bar to the left of the respective $j$.

Figure 5: Relative difference, $\delta$, of rates between the model considering the core as a homogeneous viscoelastic continuum and model VLQ. For details see Fig. 4.

Figure 6: Dependence of geocenter motion on earth-model parameters: a) motion for different lower-mantle viscosities, b) motion for different upper-mantle viscosities, c) motion for different lithosphere thicknesses. Left panels show the direction of the velocity vector projected on the Earth's surface and right panels show their amplitude, respectively.

Figure 7: Dependence of geocenter motion on different loading scenarios: a) motion for different load fractions of ICE-5G where the total mass is conserved, b) motion for different load fractions where the total mass is not conserved. Left and right panels are like in Fig. 6. In b), dashed green denotes motions due to the extended variations of ICE-5G to 0.5 to 2 for Antarctica and the yellow diamond indicates the geocenter motion where ICE5G in Antarctica is replaced by IJ05 (Ivins & James, 2005).

Figure 8: Loading history for Antarctica due to IJ05 expressed as equivalent sea level and ice mass relative to present-day ice coverage. Dashed line shows Antarctic contribution due to ICE-5G.

Figure 9: Dependence of geocenter motion on different loading scenarios but for the viscosity model VM2 with the lower mantle viscosity of $2 \times 10^{21}$ Pa s. For details see Fig. 7.

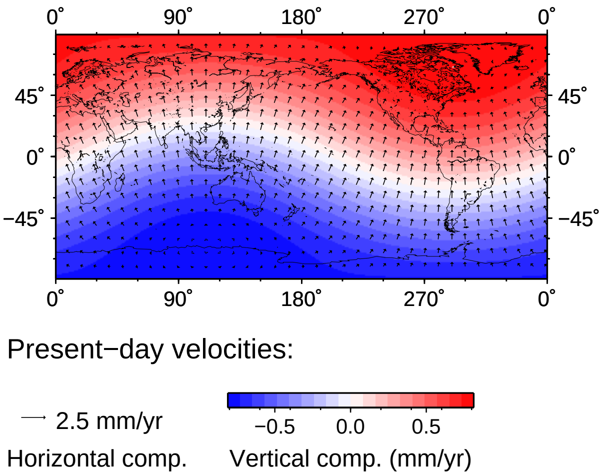
0°
90°
180°
270°
0°
45°
0°
−45°
Present−day velocities:
2.5 mm/yr
Horizontal comp.
−0.5
0.0
0.5
Vertical comp. (mm/yr)

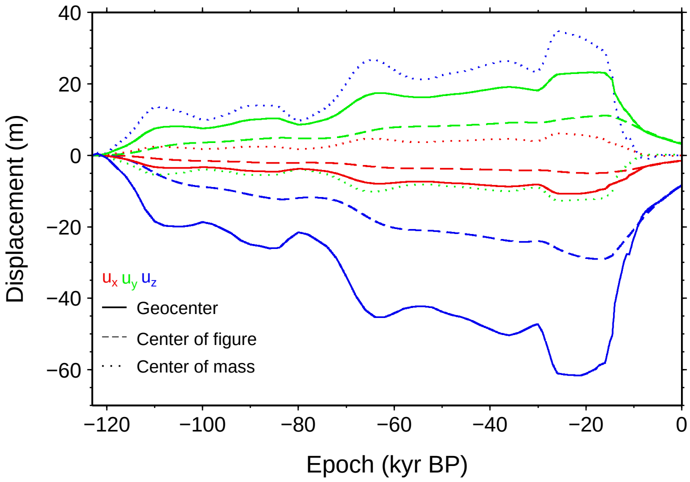

40
20
0
−20
−40
−60
Displacement (m)
−120
−100
−80
−60
−40
−20
0
Epoch (kyr BP)
u_x u_y u_z
Geocenter
Center of figure
Center of mass

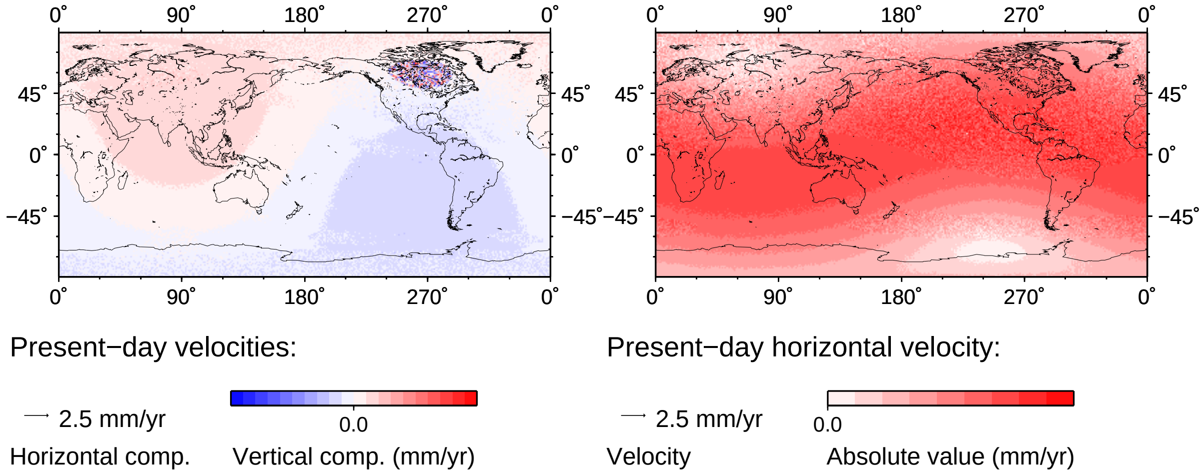

0°
90°
180°
270°
0°
45°
0°
−45°
Present−day velocities:
2.5 mm/yr
Horizontal comp.
0.0
Vertical comp. (mm/yr)
Present−day horizontal velocity:
2.5 mm/yr
Velocity
0.0
Absolute value (mm/yr)

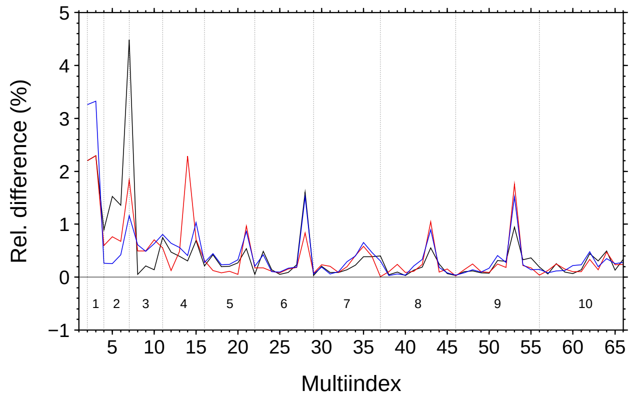

Rel. difference (%)
Multiindex
5
4
3
2
1
0
−1
5
10
15
20
25
30
35
40
45
50
55
60
65
1
2
3
4
5
6
7
8
9
10

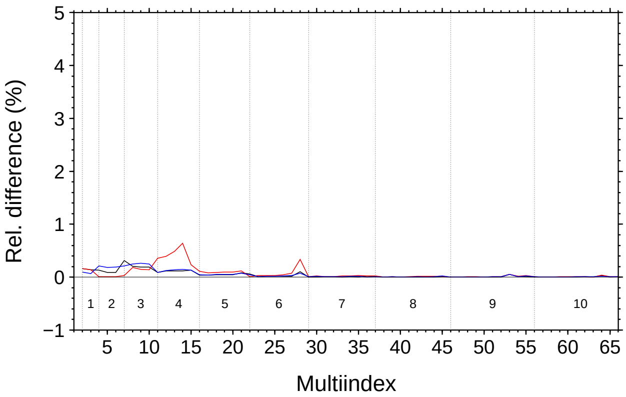

Rel. difference (%)
Multiindex
1
2
3
4
5
6
7
8
9
10

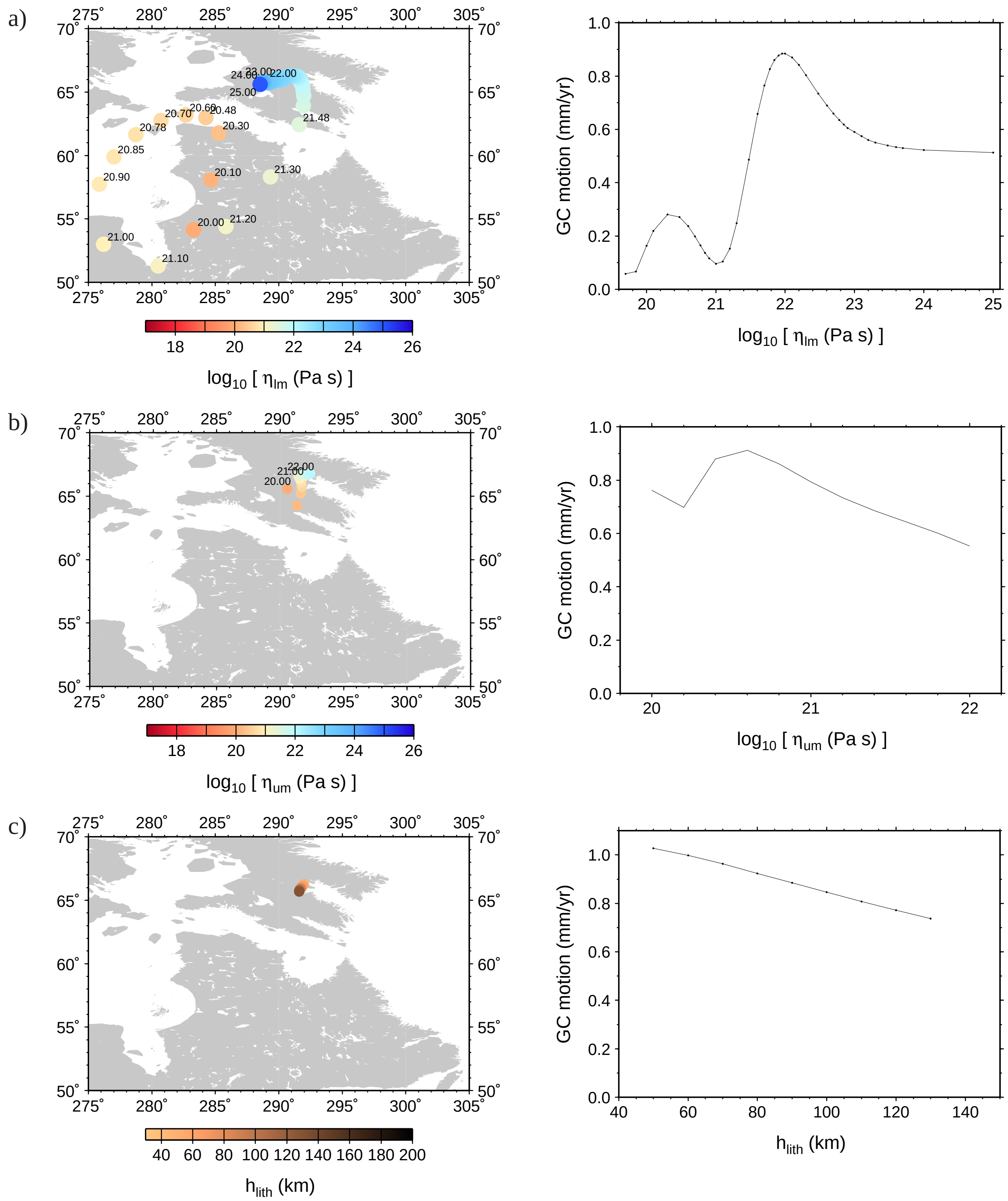
a)
24.00
23.00
22.00
25.00
20.60
20.70
20.48
20.78
20.30
21.48
20.85
20.10
21.30
20.90
20.00
21.20
21.00
21.10
log10 [ ηlm (Pa s) ]
GC motion (mm/yr)
log10 [ ηlm (Pa s) ]
b)
22.00
21.00
20.00
log10 [ ηum (Pa s) ]
GC motion (mm/yr)
log10 [ ηum (Pa s) ]
c)
hlith (km)
GC motion (mm/yr)
hlith (km)

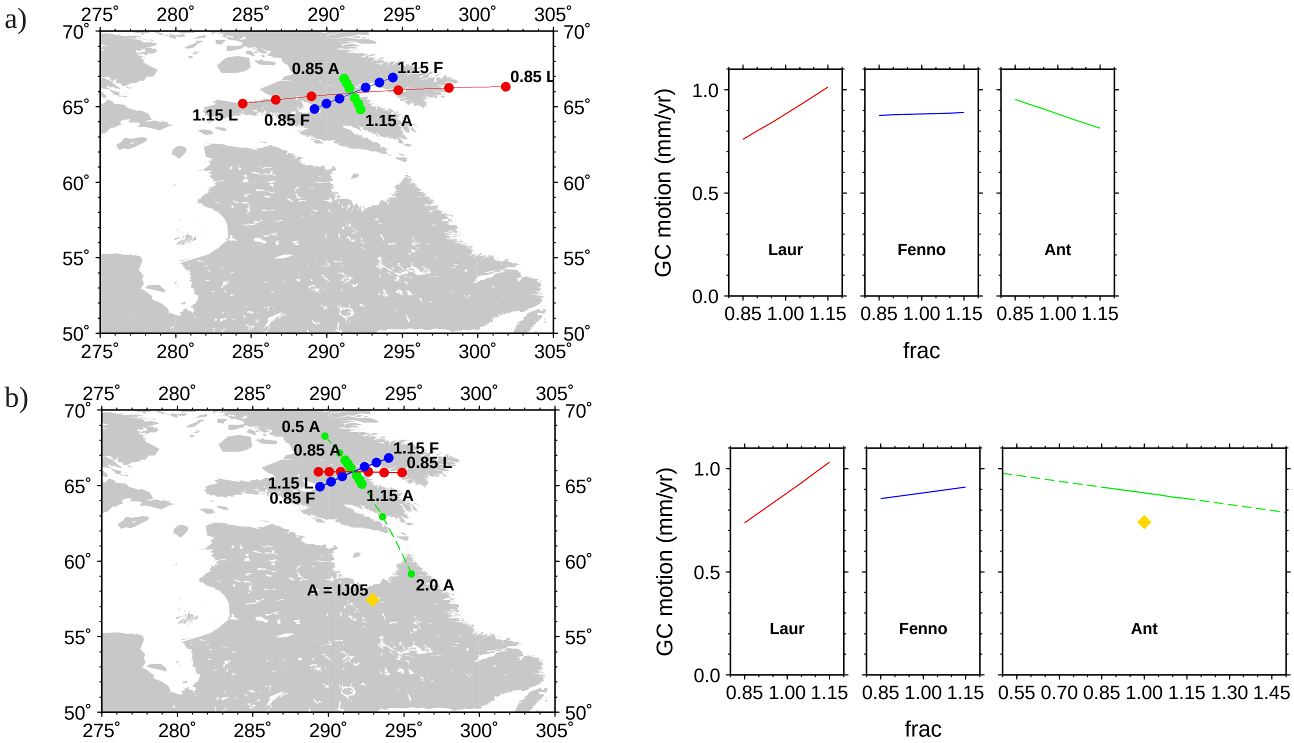

a)
0.85 A
1.15 F
0.85 L
1.15 L
0.85 F
1.15 A
GC motion (mm/yr)
Laur
Fenno
Ant
frac
b)
0.5 A
0.85 A
1.15 F
0.85 L
1.15 L
0.85 F
1.15 A
2.0 A
A = IJ05
GC motion (mm/yr)
Laur
Fenno
Ant
frac

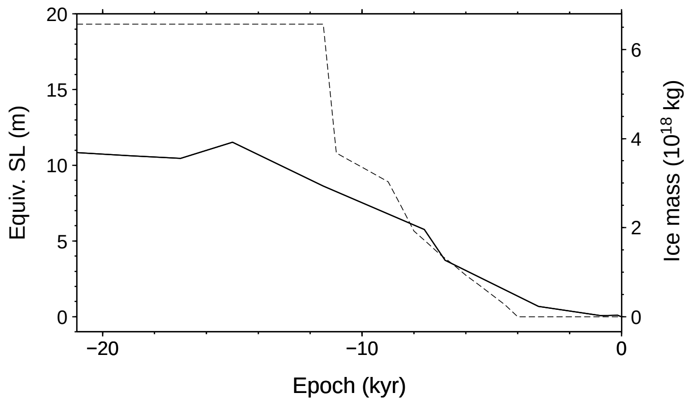

Equiv. SL (m)
Ice mass ($10^{18}$ kg)
Epoch (kyr)
20
15
10
5
0
6
4
2
0
−20
−10
0

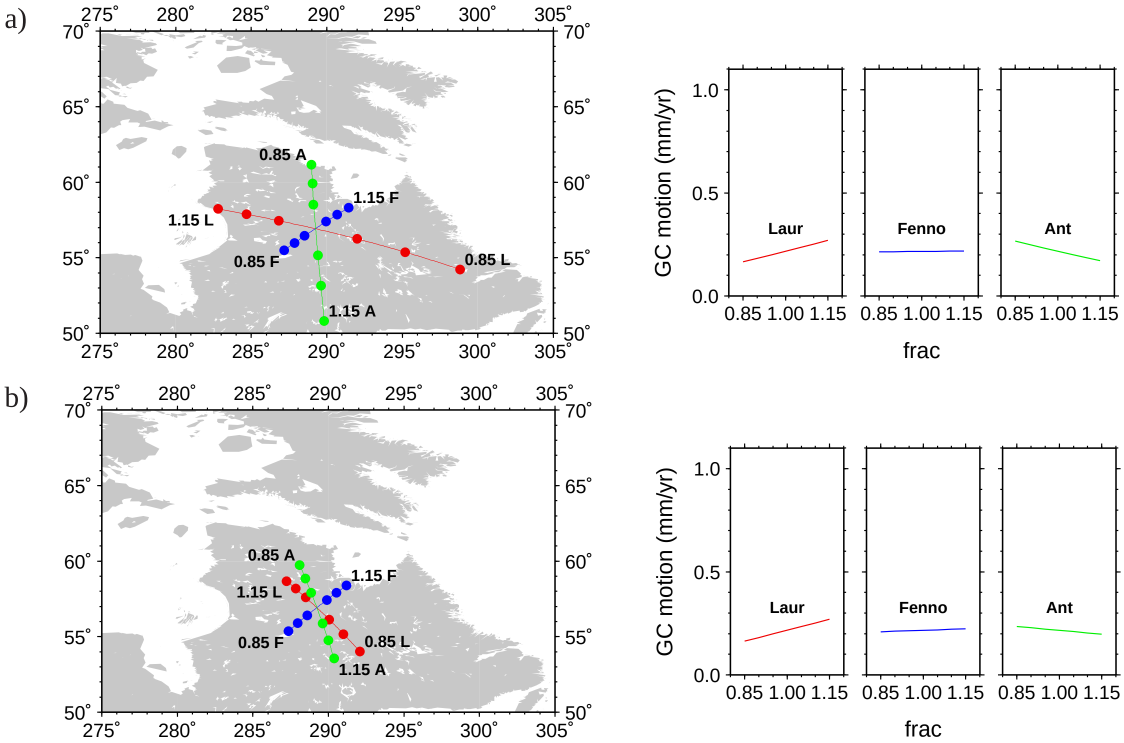
a)
b)
275° 280° 285° 290° 295° 300° 305°
70° 65° 60° 55° 50°
0.85 A
1.15 A
0.85 F
1.15 F
0.85 L
1.15 L
GC motion (mm/yr)
0.0 0.5 1.0
0.85 1.00 1.15
Laur
Fenno
Ant
frac